


Article

Design and Experiment of Electric Uncrewed Transport Vehicle for Solanaceous Vegetables in Greenhouse

Chunsong Guan ¹, Weisong Zhao ^{1,2,*} , Binxing Xu ^{1,2}, Zhichao Cui ¹, Yating Yang ¹ and Yan Gong ^{1,2}

¹ Nanjing Institute of Agricultural Mechanization, Ministry of Agriculture and Rural Affairs, Nanjing 210014, China; cs.guan@163.com (C.G.); xubinxing@caas.cn (B.X.); cuizhichao@caas.cn (Z.C.); yangyating@caas.cn (Y.Y.); gongyan@caas.cn (Y.G.)

² Western Agricultural Research Center, Chinese Academy of Agricultural Sciences, Changji 831100, China

* Correspondence: zhaoweisong@caas.cn

Abstract: Despite some rudimentary handling vehicles employed in the labor-intensive harvesting and transportation of greenhouse vegetables, research on intelligent uncrewed transport vehicles remains limited. Herein, an uncrewed transport vehicle was designed for greenhouse solanaceous vegetable harvesting. Its overall structure and path planning were tailored to the greenhouse environment, with specially designed components, including the electric crawler chassis, unloading mechanism, and control system. A SLAM system based on fusion of LiDAR and inertial navigation ensures precise positioning and navigation with the help of an overall path planner using an A* algorithm and a 3D scanning constructed local virtual environment. Multi-sensor fusion localization, path planning, and control enable autonomous operation. Experimental studies demonstrated it can automatically move, pause, steer, and unload along predefined trajectories. The driving capacity and range of electric chassis reach the design specifications, whose walking speeds approach set speeds (<5% error). Under various loads, the vehicle closely follows the target path with very small tracking errors. Initial test points showed high localization accuracy at maximum longitudinal and lateral deviations of 9.5 cm and 6.7 cm, while the average value of the lateral deviation of other points below 5 cm. These findings contribute to the advancement of uncrewed transportation technology and equipment in greenhouse applications.

Keywords: greenhouse; uncrewed; electric; transport vehicle; navigation



Academic Editor: Jerry Gao

Received: 25 November 2024

Revised: 3 January 2025

Accepted: 6 January 2025

Published: 7 January 2025

Citation: Guan, C.; Zhao, W.; Xu, B.; Cui, Z.; Yang, Y.; Gong, Y. Design and Experiment of Electric Uncrewed Transport Vehicle for Solanaceous Vegetables in Greenhouse. *Agriculture* **2025**, *15*, 118. <https://doi.org/10.3390/agriculture15020118>

Copyright: © 2025 by the authors. Licensee MDPI, Basel, Switzerland. This article is an open access article distributed under the terms and conditions of the Creative Commons Attribution (CC BY) license (<https://creativecommons.org/licenses/by/4.0/>).

1. Introduction

As a major vegetable producer, China owns an area of about 62 million mu of protected vegetable cultivation, accounting for one-third of the total vegetable production and ensuring an annual supply of vegetables. However, the current mechanization level of facility vegetables in China is only 49.8% much lower than that of grain crops, seriously restricting the development of the facility vegetable industry [1,2], among which, solanaceous vegetables and leafy vegetables are commonly planted facility vegetables. The mechanization level of leafy vegetable harvesting is relatively high, and full mechanization has basically been achieved [3]. Because solanaceous vegetables are cultivated using elevated trellises, they grow lush branches and leaves and have narrow ridges, so mechanized operations have only been achieved in some aspects such as tilling, plant protection, and water and fertilizer management. Harvesting and transportation are basically performed manually [4], which is labor-intensive and inefficient. Although there are a small number of lightweight transporters, manual operation is needed for walking, picking and loading into boxes, and transportation and unloading, with many repetitive processes and a low degree of

automation. With the urbanization process acceleration, China faces a serious problem of an aging population in agriculture, and the problems of “difficulty in employment and expensive labor” are becoming more prominent [5]. There is an urgent need to develop intelligent uncrewed transport equipment suitable for solanaceous vegetable cultivation in China.

In order to solve the transporting problem of solanaceous vegetables in greenhouses, research on automated transport vehicles or platforms in greenhouses, as well as product applications, has been ongoing globally. According to the walking mode, they can be divided into two types: with tracks and without tracks. According to the control method, they can be equipped with manual control, remote control, following, automatic operation, and other control modes [6]. Those with tracks include mechanical, electromagnetic, bar code, and other types, and can be divided into two types according to the layout position: hanging rails and ground rails [7]. Hanging rails are installed on the top of greenhouses via rails equipped with hanging hooks. Companies such as Hollandlift, Qingdao Zhengmu Farming and Animal Husbandry Technology Co., Ltd. (Qingdao City, China), and Shanghai Fengjin Intelligent Technology Co., Ltd. (Shanghai, China), have realized the remote control transportation development of agricultural materials, agricultural equipment, and fruits. Ground rails are laid between ridges (made of round pipes or angle steel), and wheeled transporters are used for inter-row picking and transportation of fruits. Due to the low equipment cost, it is now being applied in a few places across Shandong and Hebei provinces in China. However, the operating length of the vehicle is determined by the range of the laid track, and it is not very versatile. As for trackless vehicles, there are two types: wheeled and tracked transporters or platforms [8,9]. They have their own characteristics, displaying good inter-row pass ability, and strong functional extensibility and versatility. Wheeled vehicles are relatively flexible but turn at a large radius. While tracked vehicles have a small turning radius, the movement control is relatively complex.

In recent years, emerging technologies such as 5G, big data, artificial intelligence, Beidou navigation, and image recognition have rapidly progressed, and they have been integrated and applied in the research and development of agricultural machinery [10,11]. Advanced technology brings not only improved operating efficiency and accuracy of agricultural machinery but also reduced production costs. In particular, in recent years, the application of uncrewed technology has been gradually demonstrated on crops such as rice, wheat, cotton, orchards, and open field vegetables, making uncrewed farms a reality [12,13]. However, due to factors such as the steel skeleton of the greenhouse and crop coverage, there are problems with network signal interference and loss. These result in large errors in navigation and positioning accuracy, which has led to slow progress in uncrewed production in greenhouses. In order to improve the intelligent autonomy of transport vehicles, scholars have carried out some research studies. Shi Yundao et al. designed a facility sprayer chassis based on visual navigation that can flexibly turn and walk autonomously [14]; Nhu Tuong An Nguyen et al. used machine vision to autonomously navigate a facility tomato sprayer, and used a visual algorithm to determine the leaf density of tomato plants, so that pesticides can be applied as needed [15]; Li et al. found that by using high-precision geomagnetic sensors and telephoto high-resolution cameras, the navigation accuracy of large-arch greenhouse transport vehicles can be further improved [16]; and Kenan Liu et al. designed an autonomous navigation system for a greenhouse tomato-picking robot based on laser SLAM, which has shown good positioning accuracy for both straight and turning driving in 80 cm aisles [17].

In conclusion, the technical research and application of uncrewed transportation vehicles within agricultural facilities present numerous challenges. These include the intricate nature of the facility environment, the unpredictability of crop growth, the precision and

adaptability of sensor recognition, and considerations of production cost. In light of these challenges, this study introduces the design of an uncrewed transporter tailored to the structural attributes of modern continuous greenhouses and the specific agronomic practices of elevated tomato cultivation prevalent in China. The design encompasses a thorough analysis of critical components, navigation systems, and overarching control mechanisms. Subsequent to the design phase, prototype operational performance was rigorously evaluated through both bench tests and field trials. The overarching objective of this endeavor is to reduce the reliance on manual labor, particularly in addressing the laborious and costly processes associated with the unloading and frame changing of existing transport vehicles. Furthermore, the implementation of this technology aspires to enhance the level of intelligent management in the production of facility-grown vegetables.

2. Materials and Methods

2.1. Production Agronomy and Requirements

The single-span structure of the multi-span greenhouse and the planting scene of solanaceous vegetables (tomatoes as an example) are shown in Figure 1. Tomatoes are cultivated using a trough vine support system, as shown in Figure 2. The single span of the tomato is 8 m in size, with 5 cultivation slots. The width of a single cultivation slot is 0.6 m, and there is an aisle between every two cultivation slots. The aisle is a hardened road with a width of 0.9 m. There is also an aisle between the two ends of the cultivation slot and the wall, measuring 2 m. Tomatoes are planted in double rows, with the vines extending upwards and fixed in place with strings. The vines grow to a height of 1.8–2 m.

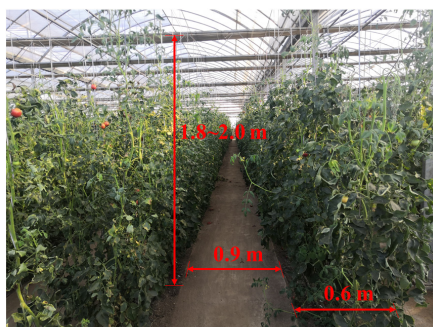


Figure 1. Scenario of tomato growing in multi-span greenhouse.

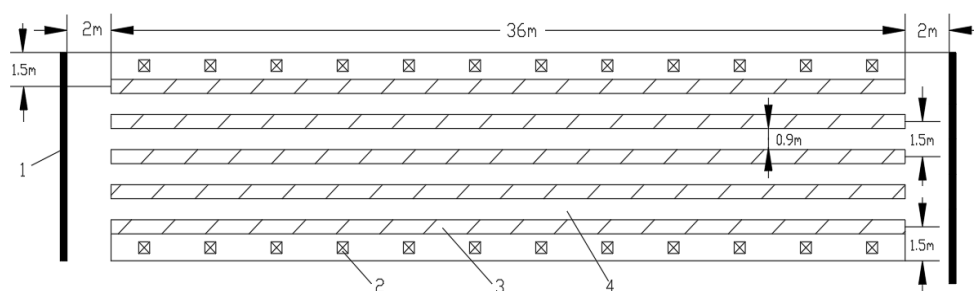


Figure 2. Top view of tomato growing scene in a unit of multi-span greenhouse: 1. Wall of greenhouse. 2. Upright column. 3. Planting rows of tomatoes. 4. Passageway.

In the context of greenhouse operations, uncrewed transport vehicles are confronted with a multifaceted driving environment. The presence of greenhouse construction materials and cultivation equipment, such as trellises, can introduce signal interferences for the machines, which poses a challenge to the navigational accuracy of these vehicles. Consequently, it is imperative that the uncrewed transport vehicles maintain adherence to their predesignated paths to minimize the risk of crop damage. This necessity is further

compounded by the constraints of the available operational space, which necessitates precise maneuvering and spatial awareness.

Therefore, to balance the carrying capacity and working flexibility of the uncrewed transportation vehicle, the overall design objectives are as follows:

Tailored to the greenhouse environment for tomato hanging cultivation, the vehicle should not be more than 0.9 m, with good stability and pass ability.

The vehicle should boast a compact structure and be cost-effective, environmentally friendly, and equipped with both manual remote control and autonomous driving capabilities. The remote control range should exceed 100 m, and autonomous driving should achieve a straight-line navigation accuracy of ± 5 cm.

It should meet the requirements for short-range transportation within the greenhouse, accommodate a minimum load of 150 kg, handle inclines up to 30° , achieve a top speed of 8 km/h, and be adept at executing differential steering turns in situ.

2.2. Overall Structure and Working Principle

As shown in Figure 3, the uncrewed transport vehicle is mainly composed of an electrically driven crawler chassis, a carrier device, an unloading mechanism, a LIDAR, an antenna, and a control system. During operations, the control system orders the track route and controls the crawler chassis to drive the whole vehicle. During traveling, the LIDAR realize the perception of the surrounding environment, including the coordinate information of the real-time position. Once the uncrewed transport vehicle is loaded with goods, a manual command is given. The vehicle automatically delivers the goods to the unloading site, where the conveyor belt of the unloading mechanism unloads the vegetable basket onto the receiving device. After the unloading is completed, it continues to return to the designated route to re-deliver the goods.

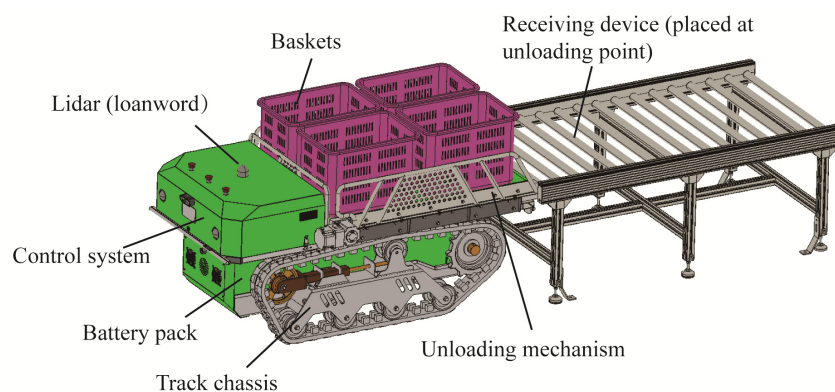


Figure 3. Simplified structure diagram of the uncrewed transport vehicle.

The main technical parameters of the uncrewed transport vehicle are shown in Table 1.

The workflow of the uncrewed transport vehicle is shown in Figure 4. The uncrewed transport vehicle starts from the starting position point P and follows the path A1, A2, A3, and A4 in sequence to the unloading point Q. Multiple stop points are set along the travel path, where the uncrewed transport vehicle halts at each stop point for a certain period of time. At this time, the vegetable farmer will pick the tomatoes near the vehicle and place them in the vegetable baskets on the vehicle. After passing through multiple stops and all the baskets on the vehicle are full of tomatoes, the vegetable farmer activates the remote control by pressing the button. Then, the vehicle automatically finds the optimal route to the unloading sites. The unloading mechanism on the vehicle operates to unload multiple vegetable baskets one by one. After completing the unloading, the vehicle moves to the

starting position P. Then, it returns to the vegetable farmer via the established walking path to initiate the next round of loading, transportation, unloading, and other actions.

Table 1. Main technical parameters.

No.	Item	Unit	Parameters
1	Dimension	Length, width, and height	1670 × 780 × 790
2	Weight	kg	250
4	Power mode	/	Dual motor drive
5	Maximum travel speed	km/h	8 (leveling limit speed)
6	Ground clearance	mm	110
7	Maximum climbing angle	°	30
8	Endurance time	h	4
9	Maximum belt load	kg	150

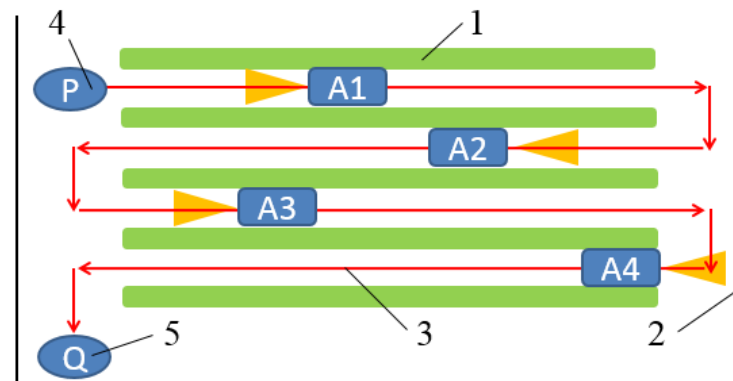


Figure 4. Workflow schematic diagram of the transport vehicle: 1. Planting rows of tomatoes. 2. Walls of the greenhouse. 3. Motion path of the transport vehicle. 4. Starting position of transport vehicle. 5. The final unloading position of transport vehicle P means that starting point Q is the unloading point. A1, A2, A3, and A4 indicate the walking paths between different cultivation tanks.

2.3. Electric Crawler Chassis Design

The electric crawler chassis is mainly composed of a lithium battery, crawler traveling motor, motor driver, transmission system, and control system. The vehicle has two traveling motors, which provide the driving force for the left- and right-side crawler traveling systems through the transmission system, respectively. The transmission system consists of a reducer, power output shaft, and chain drive mechanism. The reducer is positioned at the bottom of the vehicle with its input end linked to the motor and the output end connected to the travel system via a power output shaft and a chain drive mechanism. This design thereby enables the crawler travel system to perform the chassis’s locomotive actions. According to the overall technical parameters set, the power required by the electric crawler chassis under limited working conditions is calculated. When the vehicle is fully loaded and climbing the slope, the required power is the largest; at this time, the driving force of one side of the crawler is subjected to the force calculated in the following equation (Figure 5):

$$F = \frac{Mg \cdot \sin \theta + Mg \cos \theta (\mu_1 + \mu_2)}{2} \tag{1}$$

where M is the total mass of the uncrewed transportation vehicle climbing at the maximum angle when it is fully loaded, 400 kg; θ is the maximum climbing angle, 30°; g is the acceleration of gravity, 9.8 m/s; μ_1 is the coefficient of rolling resistance, 0.1; and μ_2 is the internal resistance coefficient, 0.05.

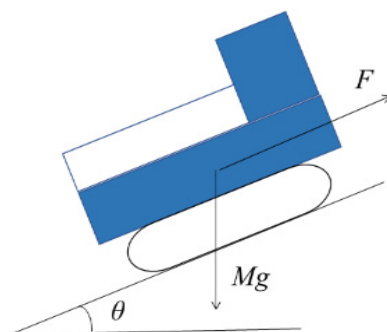


Figure 5. Force analysis diagram of full load climbing.

Then, the unilateral motor output power P is as follows:

$$P = \frac{Fv}{3.6 \times \eta} \quad (2)$$

where v is the running speed of the tracked vehicle when it climbs the slope at the maximum angle, and, here, half of the highest value of the theoretical design speed on flat ground is taken, i.e., 4 km/h; η is the efficiency of the chain drive mechanism, and it is taken as 0.95.

The power required by the unilateral motor is 1.445 kW when the uncrewed transportation vehicle is fully loaded and climbs the slope at the maximum angle. Taking into account the issues of system safety and power reserve, the left and right tracks are each equipped with a DC servo motor of type KY130ACS0425-30 as the power source of the whole vehicle. The motor is produced by Jinan Koya Electronic Science and Technology Company Limited (Jinan, China), with a rated power of 2 kW, rated voltage of 48 V, and rated speed of 3000 r/min.

According to the design requirements, it can be seen that the uncrewed transportation vehicle range time t needs to reach 4 h; then, the battery pack capacity needs to be satisfied when the cart is fully loaded:

$$Q = I_g \cdot t = \frac{I}{2} \cdot t = \frac{1}{2} \cdot \frac{2P}{U} \cdot t = \frac{P}{U} \cdot t \quad (3)$$

Here, P is the output power of one side of the motor, W; I is the normal operation of the two motors' working current, usually half of the rated current I , A; and U is the rated voltage of the motor, V.

From Equation (3), the battery pack capacity should reach 120.42 Ah. Because of the electronic motor rated voltage of 48 V, 8 single batteries of KSTAR 6-FM-65 type with a rated voltage of 12 V and rated current of 65 A are equipped (Produced by Guangdong KSTAR Industrial Technology Co., Ltd., Huizhou, China). Four of the single batteries are firstly connected in series and then connected in parallel to meet the operating requirements of motors.

2.4. Control System Design

According to the functional requirements of the uncrewed transport vehicle, it can be seen that its electronic control system needs to complete the walking power module control, unloading module control, communication control of various modules, battery power monitoring, and other functions. As shown in Figure 6, the vehicle's electronic control system is divided into three major parts with a high-voltage electric drive system design. The system also contains the vehicle controller (VCU), motor and its controller (MCU), power battery pack and its management system (BMS), and other sensing and monitoring equipment.

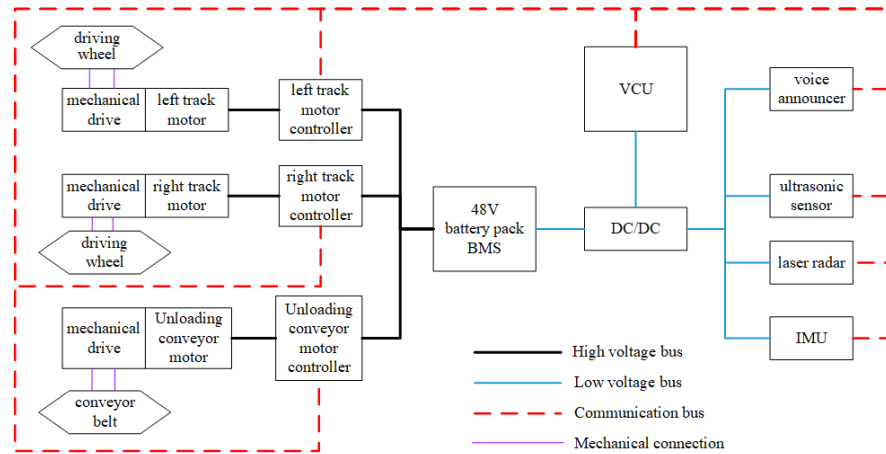


Figure 6. Overall scheme of electronic control system.

The vehicle controller is responsible for establishing seamless communication with each motor controller, the remote control system, and various sensors. It also plays a crucial role in monitoring and alerting regarding power and fault conditions. The motor control section primarily encompasses two key functionalities: walking control and unloading and conveying control.

For walking control, the system employs a dual motor drive for left and right movements. The torque and speed of the motors on both sides are independently adjustable to accommodate varying operating conditions. This allows for precise control over the vehicle’s movements, enabling it to move forward, backward, and turn through the differential control of rotational speeds.

In terms of unloading and conveying control, the unloading motor controller manages the speed of the unloading motor. The controller adjusts the motor’s running speed based on the unloading duration and the weight of the cargo, ensuring efficient and controlled unloading processes.

The uncrewed transportation vehicle deployed in the greenhouse offers dual operational modes: remote control and autonomous driving. The control flow is depicted in Figure 7. The mode is selected by adjusting the toggle switch located at the upper left corner of the remote control panel.

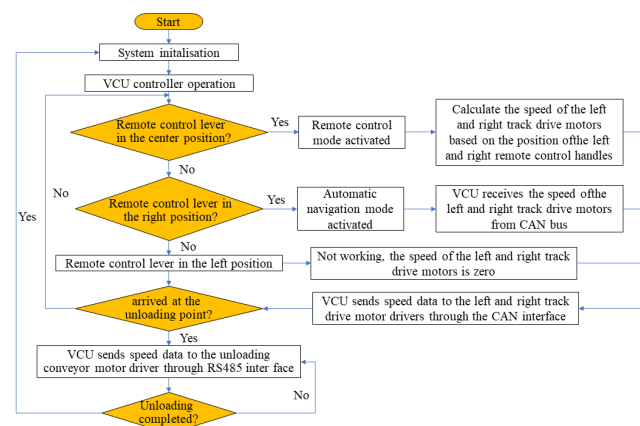


Figure 7. Control flow chart under two modes (remote control and autonomous navigation).

In the remote control mode, the toggle is set to the middle position. At this juncture, the farmer can issue operational commands based on the work site’s requirements by manipulating the left and right joysticks on the remote control. These commands are

transmitted wirelessly to the Vehicle Control Unit (VCU), which then directs the transporter to navigate freely to the designated location.

When the toggle is switched to the right position, the vehicle enters the autonomous driving mode. The Autonomous Navigation System Controller transmits signals for the left and right track drive motor speeds via the CAN bus. The VCU receives these signals for speed and forwards the data, respectively, to the left and right track motor drivers through the CAN interface to drive the transporter to operate automatically. Additionally, it assesses whether the unloading site has been reached by referencing the position coordinates, thus determining whether to initiate unloading.

Lastly, when the toggle lever is positioned to the left, the transporter remains inactive.

2.5. Design of Positioning and Navigation Systems

2.5.1. Overall Program

As designed, the uncrewed transport vehicle platform system includes a complete 3D laser SLAM system and a navigation system. The tightly coupled SLAM solution based on graph-optimized lidar (TM-LIDAR-16 from Wuhan Tianmou Optoelectronics Technology Co., Ltd., Wuhan, China) and an inertial navigation system IMU (LPMS-NAV3 series from Guangzhou Alubi Electronic Technology Co., Ltd., Guangzhou, China) constructs a 3D point cloud map of the greenhouse environment, which is then projected to a 2D raster map to provide the navigation system with a task to construct. The navigation system includes a global path-planning algorithm and a TEB path-tracking algorithm. On the constructed projected raster map, the A* algorithm is used as a global path planner to map out a safe and reliable initial path in the first instance. The path generated by the global planning is tracked by the TEB path-tracking algorithm to calculate the speed in time to complete the navigation task. The navigation system solution for the uncrewed transport vehicle is shown in Figure 8.

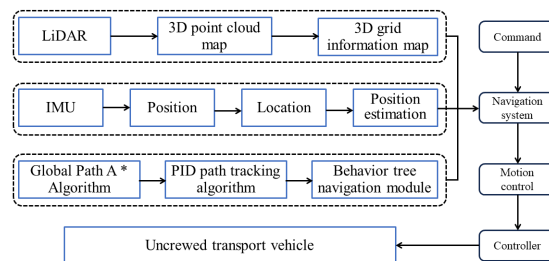


Figure 8. Overall scheme of navigation system.

The navigation task flow of the uncrewed transport vehicle is shown in Figure 9. When the uncrewed transport vehicle is moved to the starting point of the preset transport stop in the greenhouse, its current position is found by global registration with the pre-built greenhouse map. When receiving the “start task” command, the navigation system will use the preset discrete docking points as input for the global path planning module (A*). Then, a continuous trajectory is generated and passed to the local path tracking module (TEB) for trajectory tracking. The local path tracking module calculates the speed based on the robot’s current pose and the degree of overlap with the trajectory and finally generates a combined linear speed and angular speed command to be sent to the motor drive to realize the autonomous navigation function of the uncrewed transport tipper. When the TEB detects that the uncrewed transport tipper has reached each docking point, it will send a zero-speed command until it reaches the unloading point to wait for the robot to unload the goods. Then, it resumes tracking the global path after unloading is complete, thus realizing the complete operation process.

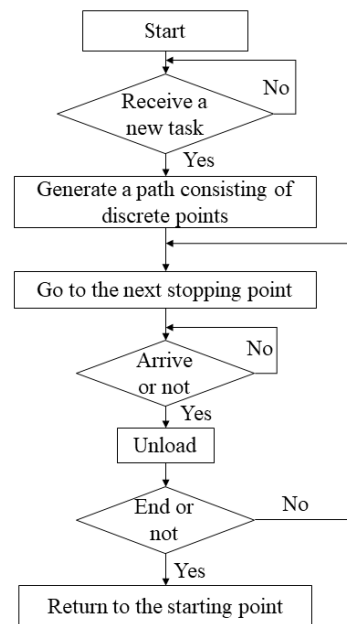


Figure 9. Navigation task flow chart.

2.5.2. Graph Optimization-Based Lidar-IMU Tightly Coupled SLAM Algorithm

Aiming at the problem that the traditional laser SLAM algorithm has certain motion estimation drift in large scene mapping, which leads to low positioning and mapping accuracy, this study adopts the tightly coupled LIDAR and inertial guidance odometry and mapping method based on graph optimization [18], and as in Figure 10, the process is divided into the following steps:

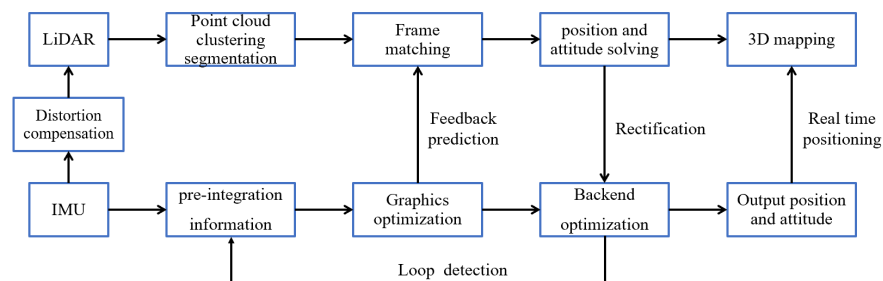


Figure 10. Lidar and inertial guidance tightly coupled odometry framework diagram.

Point cloud projection and target segmentation

The front end organizes and manages the LiDAR output point cloud data by establishing a tree structure, and then uses the high-frequency inertial guidance IMU data to correct and compensate for the aberrant point cloud of the LiDAR to offset the motion aberrations generated by the laser point cloud. After the ground point segmentation, the Breadth-First Search [19,20] (BFS) algorithm is used to cluster and segment all depth pixels on the non-ground depth map.

Feature extraction and laser odometry

Line and surface features are screened according to the neighborhood point smoothness. Ground features, line features, and surface features are matched by point and plane, point and straight line, and point and plane features, respectively. Based on the LeGO_LOAM algorithm [21,22], the nonlinear optimization equation is constructed, and the L-M algorithm is used to solve the relative position of ground features, non-ground features, and surface features step by step.

Graph optimization and 3D mapping

The back end adopts the graph optimization method to fuse the IMU pre-integration information, LiDAR odometer, and loopback detection information, and adopts the incremental smoothing and mapping (ISAM) algorithm [23] based on the factor graph optimization to carry out the overall position map optimization. Then, the back end visualizes the point cloud, the trajectory, and the constructed position map network to complete the three-dimensional map construction.

2.5.3. Path Planning Design

Path planning determines the driving range and mode of the transportation vehicle in the greenhouse, which is the premise of uncrewed operation. The quality of the path-planning algorithm directly affects the efficiency of the transportation operation. As the transportation vehicle needs to stop in the specified aisles as well as at specific points (Figure 11), in a non-open operation area, the A* algorithm [24,25] and RRT algorithm [26] applicable to discrete-point trajectory planning are selected, and the shortest distance and shortest time from the stopping point to the unloading point are taken as the goals for transportation vehicle path planning.

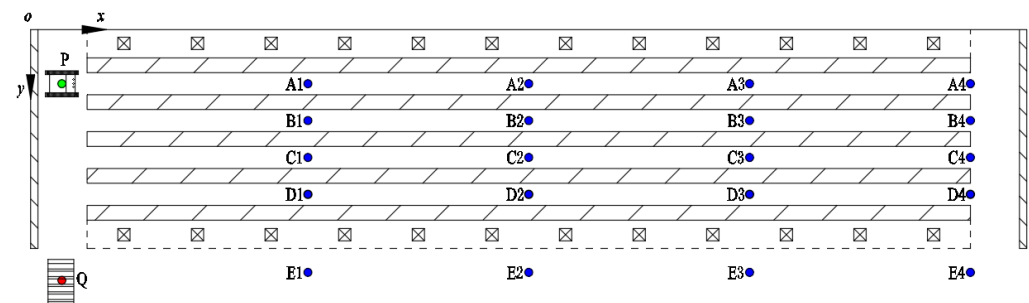


Figure 11. Running channel and stopping point position of the transportation vehicle in path planning.

The first step in path planning is to obtain environmental information by building an environment map. In static environments, a rasterization method is usually adopted. In order to better realize the rasterization, the size of each raster is adjusted to a larger size. This is needed to enlarge the actual model of the greenhouse in equal proportions. The transportation vehicle can be regarded as a mass point, while the walls, columns, and planting grooves are set to be the black part, i.e., the obstacles. The rest of the white part represents the drivable area. The green, blue, and red balls indicate the starting point, stopping point, and unloading point, respectively.

The route shown in Figure 12 was obtained through experimentation. The green, blue, and red dots in the figure indicate the starting point, characteristic stop during the work, and the unloading destination point. The red line represents the path planned by different algorithms. As can be seen from Figure 12a,b, the paths of the two algorithms are almost the same. However, the RRT algorithm significantly increases the number of nodes traversed near the stop compared to the A* algorithm [27]. The length of the RRT algorithm path is 31, which is 10 longer than the A* algorithm path for the same path. The RRT running time is 0.33 s, which is 0.26 s longer than the A* algorithm running time. The A* algorithm requires less time for path planning, has less computational complexity, and is more efficient. Therefore, considering the actual operating error, the A* algorithm is selected in this study.

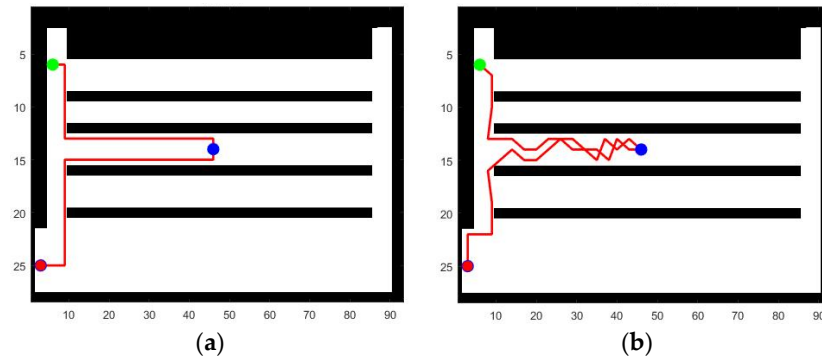


Figure 12. Experimental results of different path-planning algorithms: (a) A* algorithm and (b) RRT algorithm. The green ball indicates the starting point; the blue ball indicates the stopping point; and the red ball indicates the unloading point.

2.5.4. Path Tracking Control

The transportation vehicle is a tracked structure, which realizes the forward and backward movement of the vehicle, as well as turning in place by adjusting the speed and direction of the tracks on both sides. It is assumed that the tracked chassis is a rigid body, that the tracks do not undergo significant deformation and relative slip during movement, and that the center of mass of the vehicle coincides with its geometric center, as shown in Figure 13. The plane motion model of the transport vehicle is constructed, the ground coordinate system xoy is established, in which the instantaneous center of rotation of the transport vehicle is O_c , the forward direction is set as the positive direction of the x' -axis, and its vertical direction is set as the positive direction of the y' -axis. The running linear speed of the left and right tracks around the driving wheel is recorded as v_l and v_r , the forward speed of the geometric center of the transporter is v_c , and the x -axis direction angle is θ ; B is the center distance of the left and right tracks, and L is the grounding length of the tracks.

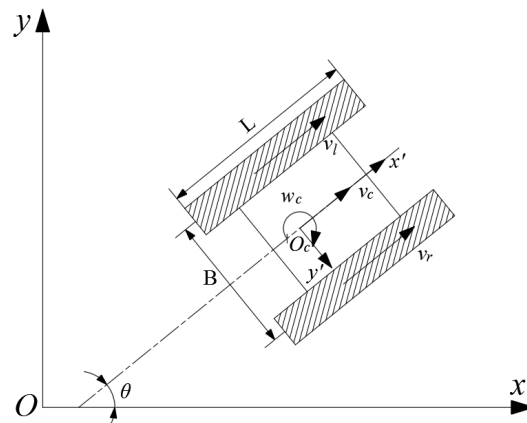


Figure 13. Kinematic model of the transporter.

The kinematic model of the transporter is given in Figure 13. It can be seen that the kinematic equations of the geometric center of the transport vehicle are as follows:

$$\begin{cases} \dot{x} = v_c \cdot \cos \theta = \frac{v_l + v_r}{2} \cdot \cos \theta \\ \dot{y} = v_c \cdot \sin \theta = \frac{v_l + v_r}{2} \cdot \sin \theta \\ \dot{\theta} = w_c = \frac{v_l - v_r}{B} \end{cases} \quad (4)$$

The integral operation of Equation (4) gives the equation of the center of mass of the transporter as follows:

$$\begin{cases} x = \frac{1}{2} \int_0^t (v_l + v_r) \cdot \cos \theta dt \\ y = \frac{1}{2} \int_0^t (v_l + v_r) \cdot \sin \theta dt \\ \theta = \frac{1}{B} \int_0^t (v_l - v_r) dt \end{cases} \quad (5)$$

Taking $x(t) = (x, y, \theta)^T$ as the state space vector, and $n(t) = (v_l, v_r)^T$ as the input vector, Equation (5) is rewritten into the state equation in matrix form:

$$\dot{x}(t) = \begin{bmatrix} \dot{x} \\ \dot{y} \\ \dot{\theta} \end{bmatrix} = \begin{bmatrix} \frac{1}{2} \cos \theta & \frac{1}{2} \cos \theta \\ \frac{1}{2} \sin \theta & \frac{1}{2} \sin \theta \\ \frac{1}{B} & -\frac{1}{B} \end{bmatrix} \cdot n(t) \quad (6)$$

From Equation (6), the center of mass of the tracked transporter is a function of the running speed of the left and right tracks, and the motion attitude at any moment can be derived from the running line speed of the left and right tracks, which is also the theoretical basis for motion control analysis of the tracked transporter.

Path tracking for the design of the controller makes the system accurately follow the planned path to arrive at the target point, which is carried out to realize the final link of autonomous walking. The PID controller has the advantages of simple algorithms, good robustness, and good reliability, is widely used in industrial control, robot control, and other industries, and has become the most commonly used method in the field of control.

The fuzzy PID control algorithm is used to limit the overshooting and stability of the system and to improve the accuracy and stability of the vehicle's automatic traveling by real-time adjustment of the control parameters k_p , k_i , and k_d (Figure 14).

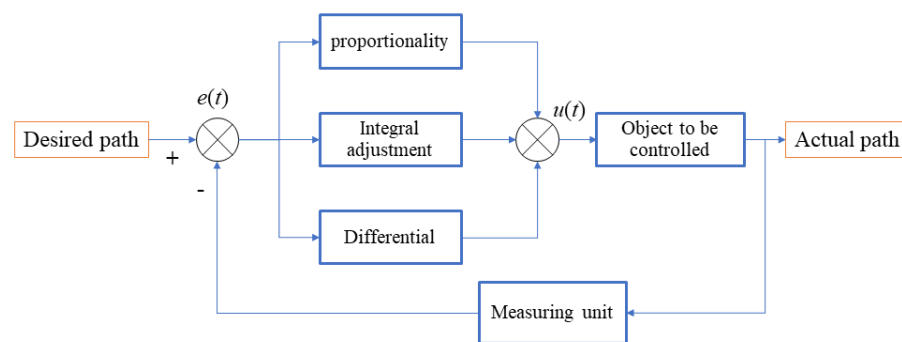


Figure 14. PID control principle diagram.

The input of the PID controller is the error signal $e(t)$. This error value is processed by ratio, integral, and differential operations to correct the deviation of the system and bring it to the desired state. In practice, it is necessary to discretize the sampled deviation and express the standard PID control output discretely with the output quantity $u(t)$ [28,29]:

$$\begin{cases} e(t) = n_0(t) - n(t) \\ u(t) = k_p e(t) + k_i \sum_{j=0}^k e(j) + k_d [e(t) - e(t-1)] \end{cases} \quad (7)$$

Here, $e(t)$ represents the deviation value, $n_0(t)$ is the desired value, and $n(t)$ is the value current actual value; k_p , k_i , and k_d represent the proportional, integral, and differential coefficients, respectively; $k_i = \frac{k_p \cdot T}{T_I}$, $k_d = \frac{k_p \cdot T_D}{T}$, and T is the sampling period, T_I is the integral time constant, and T_D is the differential time constant; $e(t)$ represents the systematic

deviation of the system at the moment of t ; and $e(t - 1)$ represents the systematic deviation of the system at the moment of $t - 1$.

For the tuning of PID parameters, this paper uses the PID Tuner toolbox in Matlab software 2018a, through which the PID controller can be efficiently designed and the parameters can be automatically adjusted to meet the required control performance of the system.

3. Experiment and Result Analysis

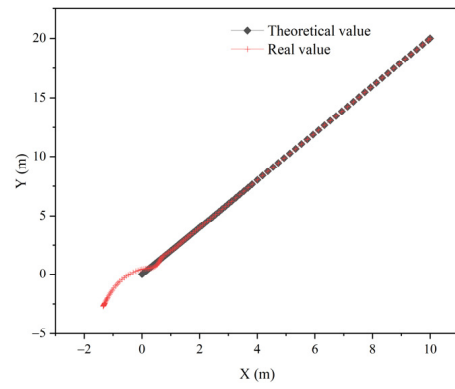
3.1. Simulation Analysis

In the Matlab simulation environment, the model of the PID control method is constructed. For the conventional PID control method, the proportional, integral, and differential parameters are determined commonly using the trial-and-error method. Finally, the parameters are determined to be $k_p = 5$, $k_i = 0.2$, and $k_d = 0.1$. In order to verify the robustness of the controller designed in this paper, the control performance of the control system under different expected trajectory changes is considered. Figure 15 shows the simulation results of the trajectory tracking of the transport vehicle under PID control. The expected trajectories in Figure 15a–c are a straight line, a curve, and a circle. It can be seen that under this design control strategy, the system output can reach the set value very well, and the adjustment time is very short throughout the process. This shows that the designed PID controller has a good system response, which can quickly adjust the system output with a small error and has a small static error after stabilization. The transport vehicle can track various trajectories (straight lines, curves, and circles) well under the action of the PID controller, adjust its position in time, and adapt to changes in various paths.

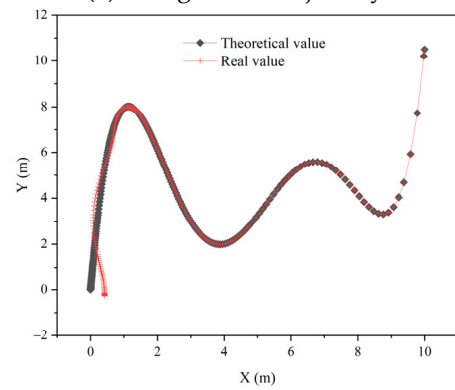
Taking the circular trajectory as an example, the initial position was set from the original $[X, Y, \text{Theta}] = [3, 0, 0]$ to $[X, Y, \text{Theta}] = [1, 1, 1]$. The simulation results are presented in Figure 16. It can be observed that the system is still capable of tracking the circular trajectory.

The errors of x , y , and θ as functions of time are extracted and depicted in Figure 17. By examining the error curves, it is evident that the system's errors remain small and eventually approach zero, indicating that the system has achieved perfect tracking of the circular trajectory. In summary, the PID trajectory tracking system designed in this paper exhibits excellent robust performance.

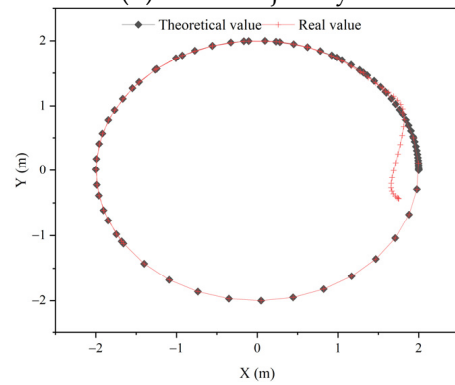
The control effect of the curve trajectory tracking of the transportation vehicle under different speeds is simulated, and the results are shown in Figure 18. As can be seen from Figure 18a, a larger initial deviation of 50 cm is defined. Under different speed conditions, the overshoot of lateral position deviation control does not change significantly. As the speed increases, the time required for the state response to reach a steady state gradually decreases. The longest time required to reach a steady state is around 2.10 s at a speed of 2 km/h. At this point, the initial deviation of 50 cm has been adjusted to only 2.3 cm. If the deviation reaches 2.3 cm at a speed of 8 km/h, it only takes 0.92 s. As can be seen in Figure 18b, with a defined initial deviation of 30° , the overshoot of heading angle deviation control varies significantly under different speed conditions. As the speed increases, the overshoot decreases significantly, and the time required to reach a steady state of about 5° is shorter. The time required to reach a steady state at a low speed of 2 km/h and a high speed of 8 km/h is 1.6 s and 0.59 s, respectively. This indicates that the designed PID controller has a good adaptive control effect on the interference of speed factors and can achieve fast and stable control.



(a) Straight-line trajectory



(b) Curve trajectory



(c) Circular trajectory

Figure 15. Tracking control results of different running trajectories of the transportation vehicle.

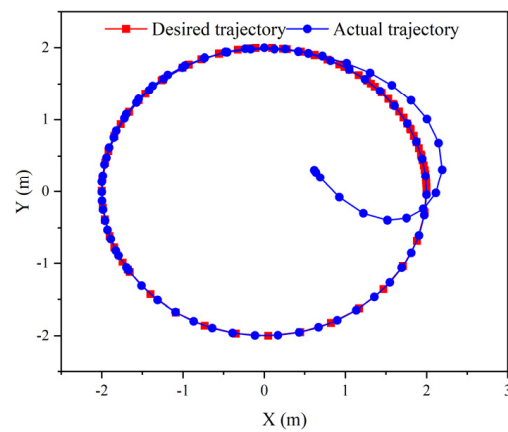


Figure 16. Circular trajectory of the PID controller with initial position change.

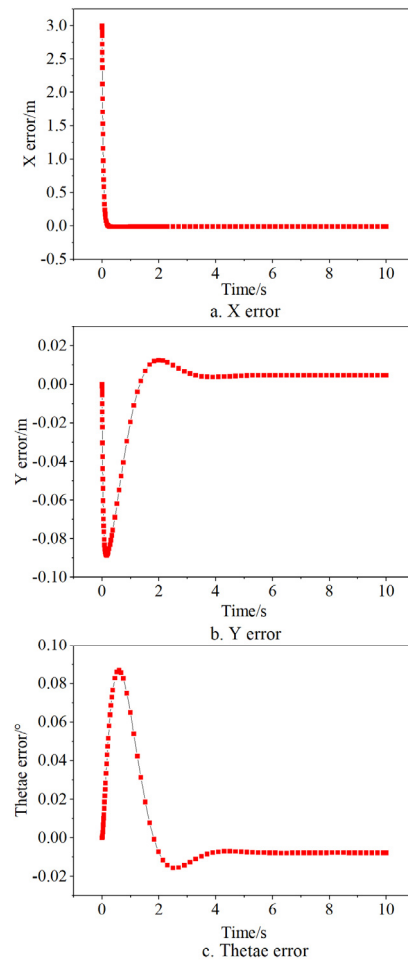


Figure 17. Error curves of the PID controller.

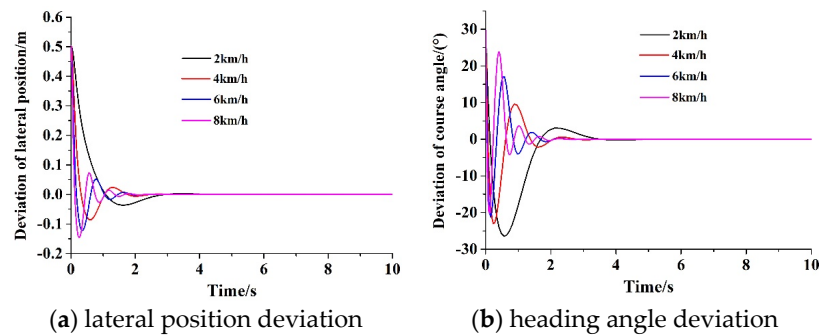


Figure 18. Tracking error of curve trajectory at different speeds.

3.2. Multi-Span Greenhouse Environment Mapping and Analysis

The use of 16-line LiDAR with a larger-ranging range solves the problem that the single-line lidar with a smaller-ranging range cannot properly construct the entire greenhouse environment in an environment with no features within the range; the LeGO_LOAM algorithm is used to build a map of the greenhouse, and the establishment of the environment map provides an accurate driving path for the movement of the cart [30,31]. As can be seen in Figure 19, the point cloud map created by the LeGO_LOAM algorithm is, overall, a square. The contours of the skeleton, columns, walls, and other parts of the continuous greenhouse are more obvious. Even after the tomato grows out, it is still possible to utilize the top of the skeleton, beams, and other structural contours to provide more accurate positioning data for navigation. This can avoid the repetitive work of constructing the same planting greenhouse several times.

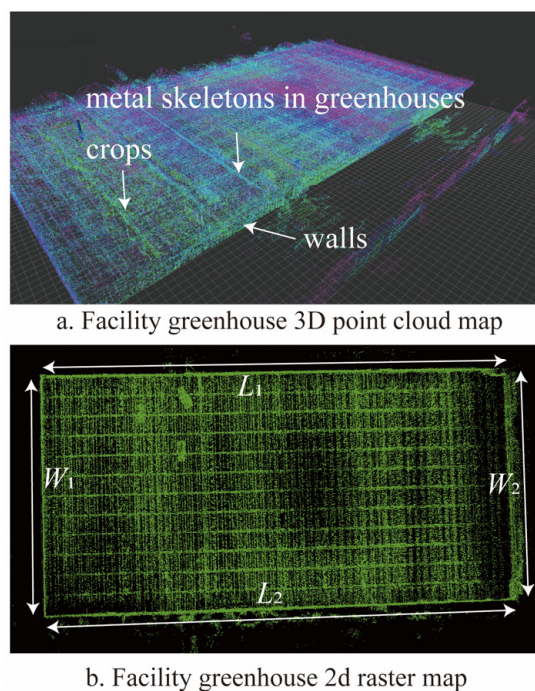


Figure 19. Virtual modeling effect diagram of the greenhouse environment.

The overall area of the greenhouse is about 3800 m² with a rectangular shape, a length of 96 m, and a width of 40 m. The dimensions of the greenhouse grid map were measured and compared with the actual data. The results are shown in Table 2. The maximum deviation between the actual dimensions and the grid map dimensions deviated by a maximum of 2.24 cm, a minimum deviation of 1.67 cm, and an average deviation of 1.94 cm. The deviations meet the mapping index of the autonomous navigation system. Meanwhile, the deviation values are very close, which proves the stability of the LeGO_LOAM algorithm.

Table 2. Map accuracy analysis of greenhouse.

Measured Points	Actual Size/cm	Map Size/cm	Absolute Error/cm
Left-side width W_1	4000	3998.32	−1.68
Front-side length L_1	9600	9597.83	−2.17
Right-side width W_2	4000	3997.76	−2.24
Rear-side length L_2	9600	9598.33	−1.67

3.3. Test Analysis

In October 2024, performance testing and verification tests of the prototype were carried out at a multi-span greenhouse base in Guli, Nanjing City, Jiangsu Province. The main tests will be the driving performance of the uncrewed transport vehicle, including tests of pass ability, stability, load-bearing performance, and trajectory tracking.

3.3.1. Transportation Performance Test

The prototype was placed in an open area on the ground and the speed performance test was conducted. The tools used for the test were a leather ruler and a stopwatch. The external environment was the same, and the stopwatch was used to record the length of time that the uncrewed vehicle traveled a 20 m distance at speeds of 0.3, 0.6, and 0.9 m/s.

Each speed was tested five times, and the average value was taken. The relative error Δ between the actual and theoretical duration was calculated as shown in Equation (8):

$$\Delta = \frac{|t - t_0|}{t_0} \times 100\% \quad (8)$$

where Δ is the relative error between the actual and theoretical durations; t is the actual duration, s; and t_0 is the theoretical duration, s.

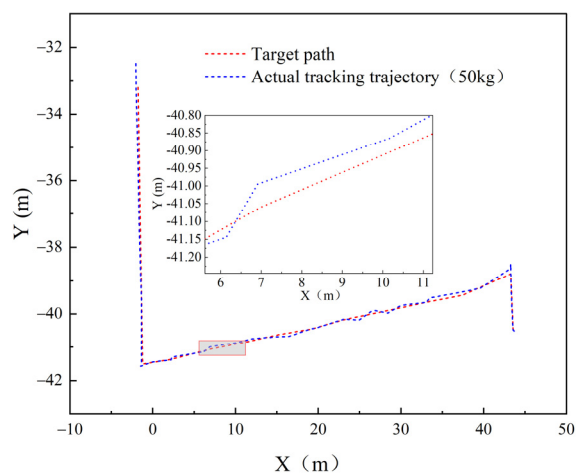
The uncrewed vehicle speed test was carried out by replacing the loaded weight on the uncrewed vehicle, and the results are shown in Table 3. It can be found that the relative error of traveling time increases with the increase in traveling speed when the load is the same. For example, the relative errors corresponding to the speeds of 0.3, 0.6, and 0.9 m/s are 0.16%, 0.66%, and 3.87%, in that order, when the load is empty. At the same traveling speed, the relative error increases with the increase in load, especially at large load conditions. The fluctuation of the relative error may be due to the differences in the starting and braking times of the uncrewed vehicle caused by the load and traveling speed under a 20 m traveling distance. Although there is a certain difference between the theoretical time and the actual time under different working conditions, the relative errors are all less than 5%. These results indicate that the actual traveling speed of the vehicle is basically the same as the set one, suggesting it has performed well in speed control. This performance makes it easy to operate with precision.

Table 3. Speed performance test results.

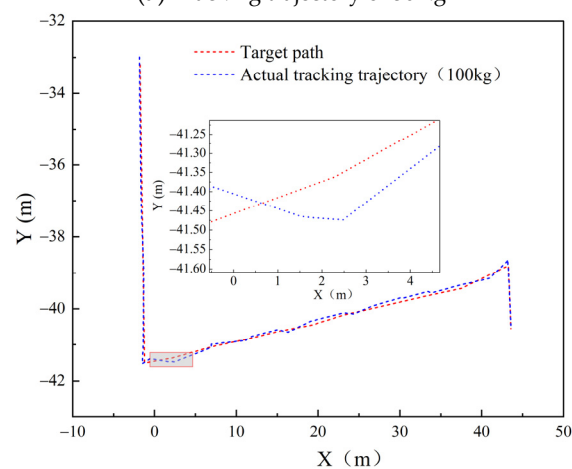
Load/kg	Speed (m·s ⁻¹)	Theoretical Time/s	Mean Value of Actual Time/s	Relative Error/%
0	0.3	66.67	66.78	0.16
	0.6	33.33	33.55	0.66
	0.9	22.22	23.08	3.87
50	0.3	66.67	66.74	0.10
	0.6	33.33	33.58	0.75
	0.9	22.22	22.95	3.29
100	0.3	66.67	66.8	0.19
	0.6	33.33	34.7	4.11
	0.9	22.22	23.21	4.46
150	0.3	66.67	67.02	0.52
	0.6	33.33	34.75	4.26
	0.9	22.22	23.32	4.95

3.3.2. Path Tracking Test

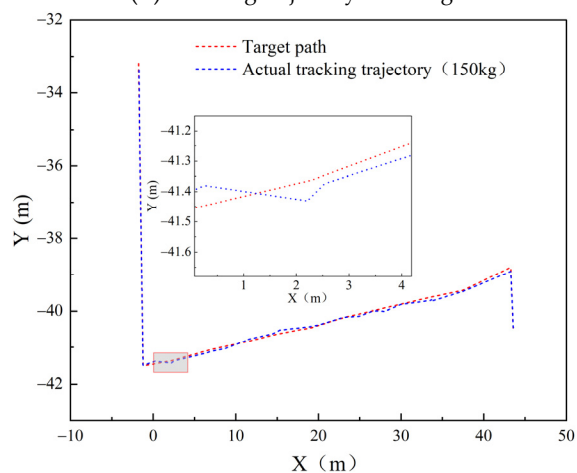
The uncrewed vehicle was loaded with 50, 100, and 150 kg and operated at a constant speed of 0.6 m/s to track the path, and the test results are shown in Figure 20. As seen in Figure 20, under different loading conditions, the actual trajectory and the target trajectory basically coincide, and the uncrewed vehicle can track the target trajectory more accurately. The largest overall lateral deviation occurs in the working area after turning, which is due to the deviation of the new starting point from the planned path caused by turning, deviating from a certain distance. By the time the uncrewed vehicle determines the pre-targeting position after path searching, the PID control is adjusted to track the preset path, and the error is continuously reduced. During traveling, the maximum track tracking error was 13.5 cm, and the average value was 6.7 cm for 50, 100, and 150 kg loads. The total width of the uncrewed vehicle's track was 70 cm, so the overall traveling on the target path did not deviate from the preset path.



(a) Tracking trajectory of 50 kg



(b) Tracking trajectory of 100 kg



(c) Tracking trajectory of 150 kg

Figure 20. Path tracking results of uncrewed vehicles with different loads.

From Figure 20, it can be found that the uncrewed vehicle has a small deviation and high tracking accuracy on the transportation path at both ends. The navigation deviation between cultivation rows (i.e., the picking area) is slightly larger; therefore, the experiment counted the deviation results of the cultivation row traveling path. The test method was as follows: set the uncrewed vehicle to travel along the cultivation rows in a straight line with maximum speeds of 0.3, 0.6, and 0.9 m/s, respectively, set one target point every 4 m, and travel a distance of 40 m. Each set of tests was repeated three times, and the lateral deviation, longitudinal deviation, and standard deviation of the uncrewed vehicle

arriving at each statistical point were recorded. The lateral deviation was positive when the actual position of the uncrewed vehicle was on the left side of the target point and negative when it was on the right side. The longitudinal deviation was positive when the uncrewed vehicle was in front of the target point and negative when it was behind the target point. The results are shown in Table 4.

Table 4. Positioning deviation.

Test Point	0.3 m/s		0.6 m/s		0.9 m/s	
	Mean Value of Lateral Deviation/cm	Mean Value of Longitudinal Deviation/cm	Mean Value of Lateral Deviation/cm	Mean Value of Longitudinal Deviation/cm	Mean Value of Lateral Deviation/cm	Mean Value of Longitudinal Deviation/cm
1	6.1 (0.21)	9.1 (0.61)	6.7 (0.29)	9.1 (0.63)	6.3 (0.29)	9.5 (1.63)
2	4.5 (0.13)	5.5 (0.33)	5.5 (0.33)	6.3 (0.53)	4.5 (0.23)	6.5 (1.08)
3	3.6 (0.20)	5.6 (1.01)	4.4 (0.22)	4.6 (0.39)	4.3 (0.32)	5.5 (0.79)
4	3.6 (0.18)	4.7 (0.78)	4.6 (0.22)	5.7 (0.73)	5.6 (0.42)	4.7 (0.77)
5	3.5 (0.33)	5.2 (0.64)	3.4 (0.23)	4.8 (0.52)	3.4 (0.23)	4.0 (0.53)
6	3.8 (0.25)	3.7 (0.32)	3.5 (0.22)	5.7 (0.62)	6.2 (0.35)	3.7 (0.67)
7	3.0 (0.18)	2.4 (0.38)	2.6 (0.20)	3.6 (0.32)	4.6 (0.26)	3.6 (0.31)
8	2.5 (0.32)	3.5 (0.34)	3.1 (0.18)	3.5 (0.32)	3.8 (0.98)	4.5 (0.57)
9	2.6 (0.24)	2.6 (0.15)	2.7 (0.15)	4.3 (0.45)	2.8 (0.77)	4.9 (0.25)
10	3.0 (0.53)	2.2 (0.13)	3.7 (0.58)	4.5 (0.33)	3.7 (0.62)	3.7 (0.36)

Note: Standard deviations are in parentheses.

By Table 4, it can be seen that the maximum positioning deviation of uncrewed vehicles at different speeds is at test point 1, with a maximum longitudinal deviation of 9.5 cm and a maximum lateral deviation of 6.7 cm. The longitudinal deviation is greater than the lateral deviation. After the second test point, both the lateral deviation and longitudinal deviation become significantly smaller. With the increase in traveling distance, the deviation becomes smaller gradually. The average value of the lateral deviation is less than 5 cm. Such high positioning accuracy can ensure that the uncrewed vehicle travels along the target trajectory.

3.4. Field Trial Validation

In October 2024, the validation test was carried out in a continuous greenhouse in Guli, Nanjing City, Jiangsu Province, China, with tomato as the planting model crop, cultivation tanks with a length of 40 m, a machine traveling roadway with a width of 0.9 m, and a cement hardened roadway. The test site is shown in Figure 21.

The straight-line speed test results showed that the speed of the transporter was 0~1.2 km/h. The turning test showed that the transporter could realize the in situ differential steering on both the concrete and the viscous ground surface. The theoretical time and the actual time were 3.2% when moving with a full load (150 kg). The validation test results are depicted in Figure 22. The longitudinal position deviation was 5.7 cm, and the lateral deviation was 4.83 cm. The range time test of the transporter was carried out, and the results showed that the range time of the transporter was 3.93 h. From the results of the field test, it can be seen that the traveling speed, minimum turning radius, unloading mechanism, and longitudinal/lateral deviation of the uncrewed transporter can meet the requirements of uncrewed transportation operation in the greenhouse environment. Therefore, it is shown that the scheme of combining LiDAR and inertial guidance adopted in this study can enable the uncrewed vehicle to maintain high localization and navigation accuracy in such a complex environment as a greenhouse.



Figure 21. Uncrewed transportation vehicle field trial.

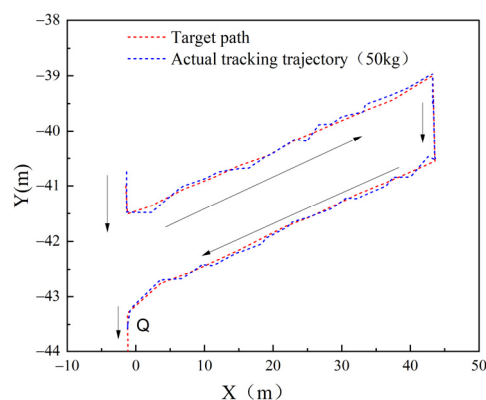


Figure 22. Uncrewed transport vehicle field validation test trajectory.

3.5. Discussion

The autonomous operation of agricultural machinery necessitates a high degree of perceptual accuracy. Numerous scholars have explored various fusion models to enhance the performance of agricultural machinery.

As shown in Table 5, satellite positioning systems such as GPS and BDS provide precise absolute positioning for uncrewed agricultural vehicles or agricultural robots with positioning errors within 2.5 cm [32,33]. Zhang et al. [34] focused their research on a rice transplanter from Kubota, employing a Real-Time Kinematic Global Positioning System (RTK-GPS) and electronic compass technology for precise positioning. Their work achieved the automated control of the transplanter along both curved and straight trajectories, with the maximum lateral deviation recorded at less than 8.7 cm when the transplanter was moving at a velocity of 0.33 m/s. Xiong [35] used the RTK-BDS positioning method based on the Beidou satellite navigation system to realize the automatic navigation and spraying operation of the orchard pesticide applicator. Meanwhile, Liu et al. [36] integrated RTK-GNSS technology into the automatic navigation system of the ZP9500 spray machine, conducting comprehensive tests across diverse environments, including cement fields, dry fields, and paddy fields. In the particularly challenging operational conditions of a paddy field, the system exhibited a maximum lateral deviation of 17.5 cm, showcasing the resilience and adaptability of the technology in complex agricultural settings.

Table 5. Comparison table of automated navigation technologies.

Key Methods	Research Object	Error Range/cm
CD + GPS [32,33]	Straight driving	2.5
RTK-GPS + Compass [34]	Kubota rice transplanter	8.7
RTK + BDS [35]	Orchard applicator	10
RTK + GNSS [36]	Test of cement, dry land, and paddy field in complex environment	17.5
UWB + IMU [37]	Strawberry plant protection robot in greenhouse	11.95
LiDAR + IMU	Test of cement in complex greenhouse environment	Maximum longitudinal and lateral deviations of 9.5 cm and 6.7 cm

It can be seen that the current level of tractor autopilot technology with John Deere and other agricultural machinery giants has reached the application level. However, in the complex operating environment, high-precision positioning and navigation technology still face serious challenges. Particularly, in the greenhouse environment, the high-precision positioning technology is still not conquered due to factors such as the influence of shading and environmental limitations. Bi et al. [37] proposed a method based on UWB ranging value correction to reach IMU-UWB fusion localization and experimentally obtained the localization error of the strawberry plant protection robot in a greenhouse as 11.95 cm. This study introduces a graph-optimized, tightly coupled laser and inertial SLAM system, LIDAR-IMU data fusion for enhanced facility navigation, achieving maximum deviations of 9.5 cm and 6.7 cm.

4. Conclusions

Given the labor-intensive nature of solanaceous vegetable production, this study introduces an electric, uncrewed transport vehicle designed for energy efficiency and environmental friendliness. It features a lightweight, compact structure and can autonomously move, stop, turn, and unload along a preset path, meeting the electric chassis performance and range specifications.

To tackle greenhouse complexities, large positioning errors, and low navigation precision of uncrewed vehicles, SLAM system based on fusion of LiDAR and inertial navigation and A* algorithms is used to ensure high-precision positioning and path tracking for uncrewed vehicles.

Transportation tests reveal that travel time relative error increases with speed at a constant load and with a load at a constant speed, especially under heavy loads. Despite theoretical and actual time discrepancies, relative errors stay under 5%, indicating close adherence to set speeds. The uncrewed vehicle closely follows the target path, with a maximum tracking error of 13.5 cm and an average of 6.7 cm. The highest positioning error is found at the initial test point 1, with a maximum longitudinal and lateral deviation of 9.5 cm and 6.7 cm, with the average value less than a 5 cm lateral deviation in other points, confirming high positioning accuracy.

Field tests confirm that its walking speed, turning radius, unloading mechanism, and deviation meet greenhouse transport needs. The LiDAR and inertial guidance combination ensures high positioning and navigation accuracy in the complex greenhouse environment.

Author Contributions: Conceptualization, C.G. and W.Z.; methodology, C.G.; software, W.Z.; validation, B.X.; formal analysis, Z.C.; investigation, Y.Y.; data curation, Y.G.; writing—original draft

preparation, C.G.; writing—review and editing, W.Z.; funding acquisition, C.G. All authors have read and agreed to the published version of the manuscript.

Funding: This research was supported by fundamental research funds from the Chinese Academy of Agriculture Science: Research and development of an unmanned transport and unloading platform between ridges for solanaceous vegetables, grant number S202317, and the National Key R&D Program of China: Innovation research and application of unmanned production technology and equipment for open field vegetables, grant number 2023YFD2001200.

Institutional Review Board Statement: Not applicable.

Data Availability Statement: The original contributions presented in the study are included in the article; further inquiries can be directed to the corresponding author.

Conflicts of Interest: The authors declare no conflicts of interest.

References

- Chen, Y.S. Development of Vegetable Mechanization in China from 2022 to 2023. *China Veg.* **2023**, *10*, 5–10.
- Wu, W.; Wang, J.; Yang, Y.; Li, D.; Li, X.; Yan, R. Analysis of the development status and mechanization trends of economic crop industry in China. *J. Chin. Agric. Mech.* **2024**, *45*, 1–13. [[CrossRef](#)]
- Jin, Y.; Xiao, H.; Cao, G. Research on status and evaluation methods of leafy vegetable mechanization production level in China. *J. Chin. Agric. Mech.* **2020**, *41*, 196–201.
- Qi, F.; Li, K.; Li, S.; He, F.; Zhou, X. Development of intelligent equipment for protected horticulture in world and enlightenment to China. *Trans. Chin. Soc. Agric. Eng.* **2019**, *35*, 183–195.
- Veeck, G.; Veeck, A.; Yu, H. Challenges of agriculture and food systems issues in China and the United States. *Geogr. Sustain.* **2020**, *1*, 109–117. [[CrossRef](#)]
- Wang, X.; Lu, W.; Chen, M.; Wang, T. Automatic Following System for Greenhouse Harvesting Transportation Based on Adaptive Pure Pursuit Model. *Nongye Jixie Xuebao/Trans. Chin. Soc. Agric. Mach.* **2016**, *47*, 8–13.
- Zou, F.; Li, J.; He, X.; Ji, M.; Yang, X. Design and experiment of self-propelled water body restoration plants harvester. *Nongye Jixie Xuebao/Trans. Chin. Soc. Agric. Mach.* **2016**, *47*, 61–66, 82.
- Xiong, J.; Li, Z.; Lin, G.; Wu, S.; Lin, D.; Li, Q.; Xiao, W. Research on AGV simulation system based on interactive control. *J. Syst. Simul.* **2021**, *33*, 657–668.
- Cui, Z.; Guan, C.; Chen, Y.; Gao, Q.; Yang, Y. Design of small multi-functional electric crawler platform for greenhouse. *Trans. Chin. Soc. Agric. Eng.* **2019**, *35*, 48–57.
- de Araujo Zanella, A.R.; da Silva, E.; Albin, L.C.P. Security challenges to smart agriculture: Current state, key issues, and future directions. *Array* **2020**, *8*, 100048. [[CrossRef](#)]
- Quy, V.K.; Hau, N.V.; Anh, D.V.; Quy, N.M.; Ban, N.T.; Lanza, S.; Randazzo, G.; Muzirafuti, A. IoT-enabled smart agriculture: Architecture, applications, and challenges. *Appl. Sci.* **2022**, *12*, 3396. [[CrossRef](#)]
- Luo, X.; Liao, J.; Hu, L.; Zhou, Z.; Zhang, Z.; Zang, Y.; Wang, P.; He, J. Research progress of intelligent agricultural machinery and practice of unmanned farm in China. *CABI Digit. Libr.* **2021**, *42*, 8–17.
- Boursianis, A.D.; Papadopoulou, M.S.; Diamantoulakis, P.; Liopa-Tsakalidi, A.; Barouchas, P.; Salahas, G.; Karagiannidis, G.; Wan, S.; Goudos, S.K. Internet of things (IoT) and agricultural unmanned aerial vehicles (UAVs) in smart farming: A comprehensive review. *Internet Things* **2022**, *18*, 100187. [[CrossRef](#)]
- LI Daoliang, L. System analysis and development prospect of unmanned farming. *Nongye Jixie Xuebao/Trans. Chin. Soc. Agric. Mach.* **2020**, *51*, 1–12.
- Nguyen, N.T.A.; Pham, C.C.; Lin, W.-C. Development of a line following autonomous spraying vehicle with Machine vision-based leaf density estimation for cherry tomato greenhouses. *Comput. Electron. Agric.* **2023**, *215*, 108429. [[CrossRef](#)]
- Li, T.; Wu, Z.; Lian, X.; Hou, J.; Shi, G.; Qi, W. Navigation line detection for greenhouse carrier vehicle based on fixed direction camera. *Nongye Jixie Xuebao/Trans. Chin. Soc. Agric. Mach.* **2018**, *49*, 8–13.
- Liu, K.; Yu, J.; Huang, Z.; Liu, L.; Shi, Y. Autonomous navigation system for greenhouse tomato picking robots based on laser SLAM. *Alex. Eng. J.* **2024**, *100*, 208–219. [[CrossRef](#)]
- Shan, T.; Englot, B.; Ratti, C.; Rus, D. Lvi-sam: Tightly-coupled lidar-visual-inertial odometry via smoothing and mapping. In Proceedings of the 2021 IEEE International Conference on Robotics and Automation (ICRA), Xi'an, China, 30 May–5 June 2021; pp. 5692–5698.
- Sihotang, J. Analysis of shortest path determination by utilizing breadth first search algorithm. *J. Info Sains Inform. Sains* **2020**, *10*, 1–5. [[CrossRef](#)]

20. Hao, L.; Wang, Y.; Bai, Y.; Zhou, Q. Energy management strategy on a parallel mild hybrid electric vehicle based on breadth first search algorithm. *Energy Convers. Manag.* **2021**, *243*, 114408. [[CrossRef](#)]
21. Wang, Z.; Liu, G. Improved LeGO-LOAM method based on outlier points elimination. *Measurement* **2023**, *214*, 112767. [[CrossRef](#)]
22. Huaman, R.; Gonzalez, C.; Prado, S. Performance evaluation of the ROS navigation stack using LeGO-LOAM. In *Proceedings of the 9th Brazilian Technology Symposium (BTSym'23)*; Springer: Cham, Switzerland, 2024; pp. 173–183.
23. Sodhi, P.; Choudhury, S.; Mangelson, J.G.; Kaess, M. ICS: Incremental constrained smoothing for state estimation. In *Proceedings of the 2020 IEEE International Conference on Robotics and Automation (ICRA)*, Paris, France, 31 May–31 August 2020; pp. 279–285.
24. Bavi, O.; Hosseininia, M.; Heydari, M.; Bavi, N. SARS-CoV-2 rate of spread in and across tissue, groundwater and soil: A meshless algorithm for the fractional diffusion equation. *Eng. Anal. Bound. Elem.* **2022**, *138*, 108–117. [[CrossRef](#)]
25. Tang, G.; Tang, C.; Claramunt, C.; Hu, X.; Zhou, P. Geometric A-star algorithm: An improved A-star algorithm for AGV path planning in a port environment. *IEEE Access* **2021**, *9*, 59196–59210. [[CrossRef](#)]
26. Marin-Plaza, P.; Hussein, A.; Martin, D.; Escalera, A.D.L. Global and local path planning study in a ROS-based research platform for autonomous vehicles. *J. Adv. Transp.* **2018**, *2018*, 6392697. [[CrossRef](#)]
27. Wang, Y.; Fu, C.; Huang, R.; Tong, K.; He, Y.; Xu, L. Path planning for mobile robots in greenhouse orchards based on improved A* and fuzzy DWA algorithms. *Comput. Electron. Agric.* **2024**, *227*, 109598. [[CrossRef](#)]
28. Zhao, Y.; Wang, J.; Cao, G.; Yuan, Y.; Yao, X.; Qi, L. Intelligent control of multilegged robot smooth motion: A review. *IEEE Access* **2023**, *11*, 86645–86685. [[CrossRef](#)]
29. Spong, M.W.; Hutchinson, S.; Vidyasagar, M. *Robot Modeling and Control*; John Wiley & Sons: Hoboken, NJ, USA, 2020.
30. Su, Y.; Wang, T.; Shao, S.; Yao, C.; Wang, Z. GR-LOAM: LiDAR-based sensor fusion SLAM for ground robots on complex terrain. *Robot. Auton. Syst.* **2021**, *140*, 103759. [[CrossRef](#)]
31. Yang, L.; Ma, H.; Nie, Z.; Zhang, H.; Wang, Z.; Wang, C. 3D LiDAR point cloud registration based on IMU preintegration in coal mine roadways. *Sensors* **2023**, *23*, 3473. [[CrossRef](#)] [[PubMed](#)]
32. Yao, Z.; Zhao, C.; Zhang, T. Agricultural machinery automatic navigation technology. *iScience* **2024**, *27*, 108714. [[CrossRef](#)] [[PubMed](#)]
33. Li, M.; Imou, K.; Wakabayashi, K.; Yokoyama, S. Review of research on agricultural vehicle autonomous guidance. *Int. J. Agric. Biol. Eng.* **2009**, *2*, 1–16.
34. Zhang, Z.G.; Luo, X.W.; Zhou, Z.Y.; Zang, Y. Design of GPS Navigation Control System for Rice Transplanter. *Trans. Chin. Soc. Agric. Mach.* **2006**, *37*, 95–97.
35. Xiong, B.; Zhang, J.X.; Qu, F.; Fan, Z.Q.; Wang, D.S.; Li, W. Navigation control system for orchard spraying machine based on Beidou navigation satellite system. *Trans. Chin. Soc. Agric. Mach.* **2017**, *48*, 45–50.
36. Liu, Z.P.; Zhang, Z.G.; Luo, X.W.; Wang, H.; Huang, P.K.; Zhang, J. Design of automatic navigation operation system for Lovol ZP9500 high clearance boom sprayer based on GNSS. *Trans. Chin. Soc. Agric. Eng.* **2018**, *34*, 15–21.
37. Bi, S.; Zhang, G.; Li, Z.; Hu, F. Positioning Method of Greenhouse Plant Protection Robot Based on Distance Measurement Value Correction. *Trans. Chin. Soc. Agric. Mach.* **2023**, *54*, 347–358.

Disclaimer/Publisher's Note: The statements, opinions and data contained in all publications are solely those of the individual author(s) and contributor(s) and not of MDPI and/or the editor(s). MDPI and/or the editor(s) disclaim responsibility for any injury to people or property resulting from any ideas, methods, instructions or products referred to in the content.